Available online at www.sciencedirect.com

SciVerse ScienceDirect

Ceramics International 39 (2013) 5137–5143

CERAMICS INTERNATIONAL

www.elsevier.com/locate/ceramint

# Polyaniline (PANI)–$Co_{0.5}Mn_{0.5}Fe_2O_4$ nanocomposite: Synthesis, characterization and magnetic properties evaluation

H. Sozeri[a,*], U. Kurtan[b], R. Topkaya[c], A. Baykal[b], M.S. Toprak[d,e]

[a]TUBITAK-UME, National Metrology Institute, PO Box 54, 41470 Gebze, Kocaeli, Turkey
[b]Department of Chemistry, Fatih University, 34500 B Çekmece-Istanbul, Turkey
[c]Department of Physics, Gebze Institute of Technology, 41400 Gebze-Kocaeli, Turkey
[d]Department of Materials and Nanophysics, KTH-Royal Institute of Technology, 16440 Kista-Stockholm, Sweden
[e]Department of Materials Science and Engineering, Yildirim Beyazit University, Ulus-Ankara, Turkey.

Received 28 November 2012; received in revised form 3 December 2012; accepted 3 December 2012
Available online 10 December 2012

**Abstract**

Polyaniline (PANI)/Cobalt-manganese ferrite, (PANI)/$Co_{0.5}Mn_{0.5}Fe_2O_4$, nanocomposite was synthesized by oxidative chemical polymerization of aniline in the presence of ammonium peroxydisulfate (APS). Microwave assisted synthesis method was used for the fabrication of core $CoFe_2O_4$ nanoparticles. The structural, morphological, thermal and magnetic properties of the nanocomposite were investigated in detail by X-ray diffraction (XRD), fourier-transform infrared spectroscopy (FT-IR), thermogravimetric analysis (TGA), scanning electron microscopy (SEM) and vibrating sample magnetometer (VSM). The average crystallite size of (PANI)/$Co_{0.5}Mn_{0.5}Fe_2O_4$ nanocomposite by the line profile method was $20 \pm 9$ nm. The magnetization measurements revealed that (PANI)/$Co_{0.5}Mn_{0.5}Fe_2O_4$ nanocomposite has superparamagnetic behavior with blocking temperature higher than 300 K. The saturation magnetization of the composite is considerably low compared to that of $CoFe_2O_4$ nanoparticles due to the partial replacement of $Co^{2+}$ ions and surface spin disorder. As temperature decreases, both coercivity and strength of antiferromagnetic interactions increase which results in unsaturated magnetization of the nanocomposite.


*Keywords:* Magnetic nanomaterials; Coercivity; Superparamagnetism; Polyaniline

## 1. Introduction

Recently, inorganic–organic nanocomposites with controllable electric and magnetic properties have attracted increasing attention because of their unique magnetic, electrical and optical properties and their potential application in electric catalysis, chemical sensors, electromagnetic interference shielding, microwave absorption materials and photoelectric devices [1–8].

For these purposes, spinel ferrites are widely studied because of their interesting magnetic properties as well as extensive potential applications in biomedical, magnetic recording media, soft magnetic materials and absorbing materials [9–11].

In order to change the magnetic properties, substitution of other elements such as manganese into cobalt ferrites was proposed by many researchers [12–15] reported that thin films and fine particles of the manganese doped cobalt ferrites were found to be suitable for magneto-optical applications.

Among the known conducting polymers, polyaniline (PANI) is regarded as the most promising polymer for the fabrication of inorganic–organic nanocomposites because of its low cost, easy preparation, and high conductivity [16,17]. It has many potential applications in electromagnetic shielding, anticorrosion, electrode materials for secondary batteries, electrical condenser, catalysis and sensors [18–20].

Till now, many nanocomposites with PANI and spinel magnetic nanoparticles have been synthesized, such as Singh et al. [22] reported the synthesis of conducting

*Corresponding Author. Tel.: +90 262 679 5000; fax: +90 262 679 5001.
*E-mail address:* huseyin.sozeri@tubitak.gov.tr (H. Sozeri).

0272-8842/$ - see front matter © 2012 Elsevier Ltd and Techna Group S.r.l. All rights reserved.
http://dx.doi.org/10.1016/j.ceramint.2012.12.009

PANI–($\gamma$-$Fe_2O_3$) nanocomposite. Li et al. [21] also reported that $Cu_{0.4}Zn_{0.6}Cr_{0.5}Sm_{0.06}Fe_{1.44}O_4$/PANI nanocomposites showed soft magnetic character. Conductive polyaniline (PANI)–manganese ferrite ($MnFe_2O_4$) nanocomposites also have synthesized with core–shell structure by in-situ polymerization in the presence of dodecylbenzenesulfonic acid by Hosseini et al. [23]. Core–shell $Co_{(1-x)}Ni_xFe_2O_4$/polyaniline nanoparticles have been synthesized by the combination of sol–gel process and in-situ polymerization methods by Lee et al. [24]. Yuan et al. [26] synthesized the $(Sr(ZnZr)_x Fe_{12-2x}O_{19}$–PANI, $x=0.0$, 0.5, 1.0) composite through oxidative chemical polymerization of aniline and other studies [11,24–29].

In this study, PANI/$Co_{0.5}Mn_{0.5}Fe_2O_4$ nanocomposite was prepared by in situ polymerization. This is the first study for the synthesis of PANI/$Co_{0.5}Mn_{0.5}Fe_2O_4$ nanocomposite. Here, polyaniline (PANI) was used as the conducting shell. The sample was characterized by various experimental techniques (Fourier transform infrared spectrometry (FT-IR), X-ray diffraction (XRD), Scanning electron microscopy (SEM), thermal gravimetric analysis (TG) and the magnetic properties of the nanocomposite were investigated by Vibrating sample magnetometer (VSM).

## 2. Experimental

### 2.1. Chemicals and instrumentations

All chemicals including cobalt nitrate hexahydrate; $Co(NO_3)_2 \cdot 6H_2O$, iron nitrate nonahydrate; $Fe(NO_3)_3 \cdot 9H_2O$, manganese nitrate hexahydrate; $Mn(NO_3)_2 \cdot 6H_2O$, aniline; $C_6H_5NH_2$, citric acid; $C_6H_8O_7$ were obtained from Merck and used as received, without further purification.

X-ray powder diffraction (XRD) analysis was conducted on a Rigaku Smart Lab Diffractometer operated at 40 kV and 35 mA using Cu $K_\alpha$ radiation.

Fourier transform infrared (FT-IR) spectra were recorded in transmission mode (Perkin Elmer BX FT-IR) on powder samples that were ground with KBr and compressed into a pellet. FT-IR spectra in the range 4000–400 $cm^{-1}$ were recorded in order to investigate the nature of the chemical bonds formed.

The thermal stability was determined by thermogravimetric analysis (TGA, Perkin Elmer Instruments model, STA 6000). The TGA thermograms were recorded for 5 mg of powder sample at a heating rate of 10° C/min in the temperature range of 30° C–800° C under nitrogen atmosphere.

Scanning Electron Microscopy (SEM) analysis was performed, in order to investigate the microstructure of the sample, using FEI XL40 Sirion FEG Digital Scanning Microscope. Samples were coated with gold at 10 mA for 2 min prior to SEM analysis.

The magnetization measurements were performed by using vibrating sample magnetometer (VSM, Quantum Design, PPMS 9 T) in an external field up to 90 kOe in the temperature range of 10–400 K.

The variation of magnetization with temperature was investigated by measuring ZFC and FC magnetization curves of the nanocomposite samples. In a ZFC measurement, the sample is cooled from room temperature to 5 K without any external magnetic field. After the application of the field, magnetization of the sample is measured during heating the sample. In a FC measurement, the sample is initially cooled to 5 K under the applied magnetic field. Then, magnetization was measured during warming the sample from 5 to 400 K.

### 2.2. Synthesis

#### 2.2.1. Synthesis of $Co_{0.5}Mn_{0.5}Fe_2O_4$ nanoparticles

PANI/$CoFe_2O_4$ nanocomposites were prepared via an in situ polymerization of aniline in aqueous solution containing $CoFe_2O_4$ nanoparticles. $Co(NO_3)_2 \cdot 6H_2O$, $Mn(NO_3)_2$ $6H_2O$, $Fe(NO_3)_3$ $9H_2O$, citric acid and were used as reactants. The molar ratio of $Co^{2+}$, $Ni^{2+}$, $Fe^{3+}$ and citric acid were controlled at 0.5:0.5:1:1. Stoichiometric amount of metal nitrates and citric acid were ground together in agate mortar then heated in domestic MW (Arçelik mark, 2.450 GHz) oven for 4 min. The final powder was obtained.

#### 2.2.2. Synthesis of (PANI)/$Co_{0.5}Mn_{0.5}Fe_2O_4$ nanocomposite

In order to improve the contacts between $Co_{0.5}Mn_{0.5}Fe_2O_4$ nanoparticles and anilines in aqueous solution, $Co_{0.5}Mn_{0.5}$-$Fe_2O_4$ nanoparticles was dispersed in deionized water by ultrasonic waves with oscillation frequency of 40 kHz for 1 h before polymerization. 0.15 g $Co_{0.5}Mn_{0.5}Fe_2O_4$ NPs were mixed in 70 mL 1 M HCl and required amount of aniline was added slowly. Then an aqueous solution of $(NH_4)_2S_2O_8$ (APS, 2.25 g dissolved in 30 mL 1 M HCl) was added drop by drop to the above reactant mixture with stirring for 6 h at around 0° C in an ice-bath. The obtained dark-green solid was filtered, washed thoroughly with ethanol and distilled water, respectively, and dried at 70° C for 24 h in vacuum to obtain green–black powders Scheme 1.

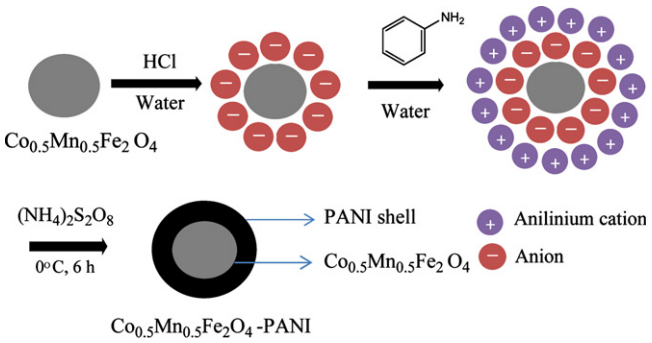


Scheme. 1. Synthesis of PANI/$Co_{0.5}Mn_{0.5}Fe_2O_4$ nanocomposite.

## 3. Results and discussion

### 3.1. XRD analysis

XRD patterns of PANI, and PANI/$Co_{0.5}Mn_{0.5}Fe_2O_4$ nanocomposite are shown in Fig. 1. The XRD pattern of as prepared PANI/$Co_{0.5}Mn_{0.5}Fe_2O_4$ nanocomposite matches with JCPDS file no 22-1086 (for $CoFe_2O_4$) and 73-1964 (for $MnFe_2O_4$) and the particles show cubic crystal structure. This indicates that the product consists of crystalline single-phase $Co_{0.5}Mn_{0.5}Fe_2O_4$ NPs. The XRD pattern of PANI (Fig. 2(a)) shows that PANI has partly crystalline structure and the two broad peaks are observed at $2\theta = 20.41^\circ$ and $25.61^\circ$ due to the densely packed phenyl rings and thus an extensive interchain pi–pi orbital overlap [29,30–33]. The mean size of the crystallites was estimated from the diffraction pattern by line profile fitting method using the equation (1) given in Ref. [32,33].

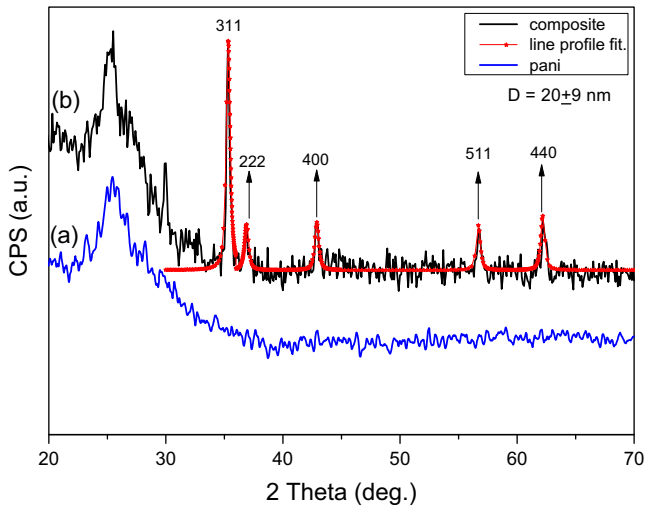


Fig. 1. XRD powder patterns of (a) PANI and (b) PANI/$Co_{0.5}Mn_{0.5}Fe_2O_4$ nanocomposite.

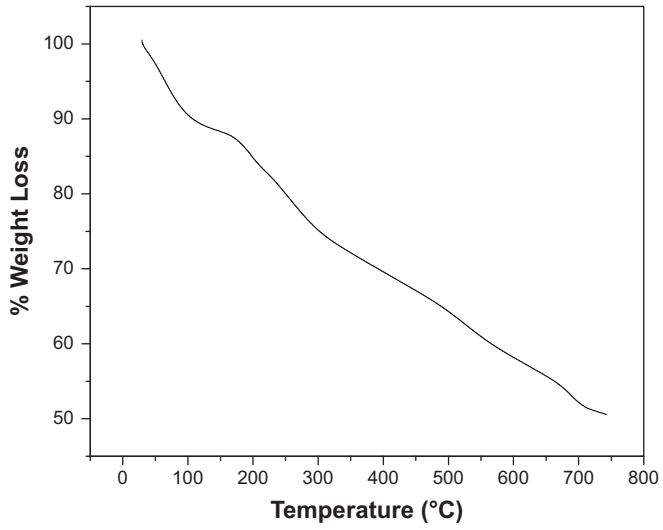


Fig. 2. TG thermogram of PANI/$Co_{0.5}Mn_{0.5}Fe_2O_4$ nanocomposite.

The line profile, shown in Fig. 1 was fitted for observed five peaks with the following miller indices: (311), (222), (400), (511) and (440). The average crystallite size was obtained as $20 \pm 9$ nm as a result of this line profile fitting.

### 3.2. TG analysis

TG thermogram of PANI/$Co_{0.5}Mn_{0.5}Fe_2O_4$ nanocomposite is given in Fig. 2. PANI shows three-step weight loss behavior which was described elsewhere [30,31,34–36]. PANI/$Co_{0.5}Mn_{0.5}Fe_2O_4$ nanocomposite undergoes similar decomposition steps as that of PANI but it has greater stability. The initial weight loss up to 105° C is due to residual water, and decomposition of PANI started after 300° C. The greater stability of composite may be due to the interaction between PANI and $Co_{0.5}Mn_{0.5}Fe_2O_4$ NPs which restricts the thermal motion of PANI chain in the composite and enhanced the thermal stability of the composite. This thermal behavior confirmed that weight percentage of PANI and $Co_{0.5}Mn_{0.5}Fe_2O_4$ NPs (organic and inorganic content) in nanocomposite as 47 and 53 respectively.

### 3.3. FT-IR analysis

The FT-IR spectra of PANI and PANI/$Co_{0.5}Mn_{0.5}Fe_2O_4$ nanocomposite are shown in Fig. 3a and b respectively. In Fig. 3a the peaks at 3419 $cm^{-1}$, 1560/1475 $cm^{-1}$, 1290 $cm^{-1}$, 1128 $cm^{-1}$ are attributed to the N–H stretching vibration, C=C stretching vibration of the quinone (Q) ring and benzene (B) ring, N–H bending stretching of the benzenoid ring, C–H in-plane bending vibration, respectively [8,26]. In Fig. 3b the absorption peaks at 3445 $cm^{-1}$, 1575/1485 $cm^{-1}$, 1297 $cm^{-1}$, and 1128 $cm^{-1}$ can also be attributed to the PANI. The FT-IR absorption of these functional groups are different in PANI and the nanocomposite. These difference in wave numbers are explained by Zhang and Yang [11] as these peaks have displayed

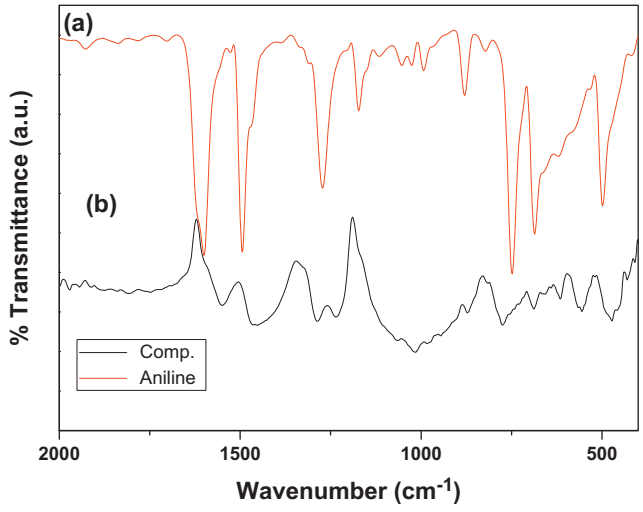


Fig. 3. FT-IR spectra of (a) PANI and (b) PANI/$Co_{0.5}Mn_{0.5}Fe_2O_4$ nanocomposite.

red-shift, due to the interactions between magnetic nanoparticles and PANI, the interaction between the N–H, C–N and the N–Q–N bonds weaken. In addition, the absorption at 460 $cm^{-1}$ is octahedral stretching vibration ($\nu_2$), of M–O and the peaks at 572 $cm^{-1}$ is due to the tetrahedral M–O stretching, vibration ($\nu_1$), of the spinel structure of $Co_{0.5}Mn_{0.5}Fe_2O_4$. All these results also showed that the synthesized nanocomposite consisted of PANI and $Co_{0.5}Mn_{0.5}Fe_2O_4$ NPs and there are intermolecular interactions between them [8,26,37].

### 3.4. SEM analysis

The morphology of the as-prepared PANI/$Co_{0.5}Mn_{0.5}Fe_2O_4$ nanocomposite was determined by scanning electron microscopy (SEM) and few micrographs are presented in Fig. 4. Globular agglomerates are observed with much finer internal structure. PANI layers may have wrapped on the surface of $Co_{0.5}Mn_{0.5}Fe_2O_4$ NPs, forming these agglomerated globules. A closer examination of these primary structures indicate nearly spherical particles with average particle size of 25 nm. When compared with the crystallite size estimated from X-ray line profile fitting, the observed nanoparticles may have nearly single crystalline character.

### 3.5. Magnetic characterization

Magnetic characterization of the composite as performed by measuring M–H hysteresis curves at different temperatures from 400 K to 10 K. Field cooled and zero field cooled (FC and ZFC) magnetization curves are presented in Fig. 5 and 6 respectively.

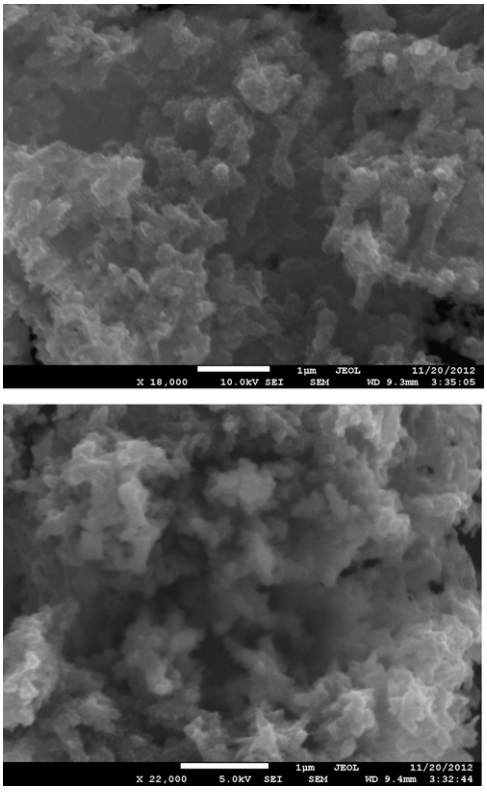


Fig. 4. SEM micrographs of PANI/$Co_{0.5}Mn_{0.5}Fe_2O_4$ nanocomposite at different magnifications.

At 400 K, magnetization of the composite shows no hysteresis with saturation magnetization, $M_s$, of ~4 emu/g. As the nanocomposite contains 53% by weight the ferrite phase, $M_s$ becomes 7.5 emu/g when normalized for the inorganic content. This value is very weak as compared to magnetization of bulk $CoFe_2O_4$ particles that is 80 emu/g [38]. Co-ferrite has an inverse spinel structure in the form of $[Co_\delta Fe_{1-\delta}]_A[Co_\delta Fe_{1+\delta}]_B O_4$ [39] where A and B corresponds to the tetrahedral and octahedral sites, respectively. $\delta$ is the inversion parameter and the case $\delta=1$ corresponds to a normal spinel structure like $ZnFe_2O_4$. In the other extreme case, i.e., $\delta=0$, structure becomes inverse spinel and typical example is $CoFe_2O_4$. In the spinel ferrites, the magnetic order is mainly due to a super exchange interaction mechanism occurring between the metal ions in the A and B sublattices. The partial replacement of $Co^{2+}$ ions with $Mn^{2+}$ ones, which has a preferential B site occupancy, results in the reduction of the exchange interaction between A and B sites. This results in a reduction in magnetization. In addition, formation of dead layer on the surface due to large surface-to-volume ratio and existence of random canting of particle surface spins at the surface [40,41] might also be the cause for the reduction of magnetization of nanoparticles. At temperatures below 100 K, magnetization of the sample does not reach to a saturation probably due to the antiferromagnetic interactions which becomes stronger at low temperatures [42].

A typical temperature dependency of the magnetization of ferrite nanoparticles are shown in Fig. 6a and b. Magnetic particles below a certain size display superparamagnetic characteristics. In very small particles, the anisotropy energy, $K_{eff}V$ of a particle of volume $V$ and effective anisotropy constant $K_{eff}$, creates a barrier for the orientation of the total magnetic moment toward the applied field.

There is also thermal energy trying to destroy magnetization of the moments which can be expressed by the equation $K_{eff}V=25\,k_BT$ where $k_B$ and $T$ are the Boltzmann constant and temperature of the system, respectively. In the ZFC curve, the temperature at which magnetization becomes maximum is called as Blocking Temperature ($T_B$), below which the free rotation of magnetic moments is blocked by anisotropy, and above $T_B$, the thermal energy is sufficient for the moments to be free and the system to become superparamagnetic. Magnetic hysteresis is observed below the blocking temperature for the superparamagnetic nanoparticles.

The ZFC and FC magnetizations in Fig. 6a and b show an irreversible magnetic behavior in the whole temperature range indicating the presence of nanoparticles in a magnetically blocked state still at room temperature. In the absence of interparticles interactions, the temperature at which the two curves (ZFC and FC curves) separate ($T_{sep}$)

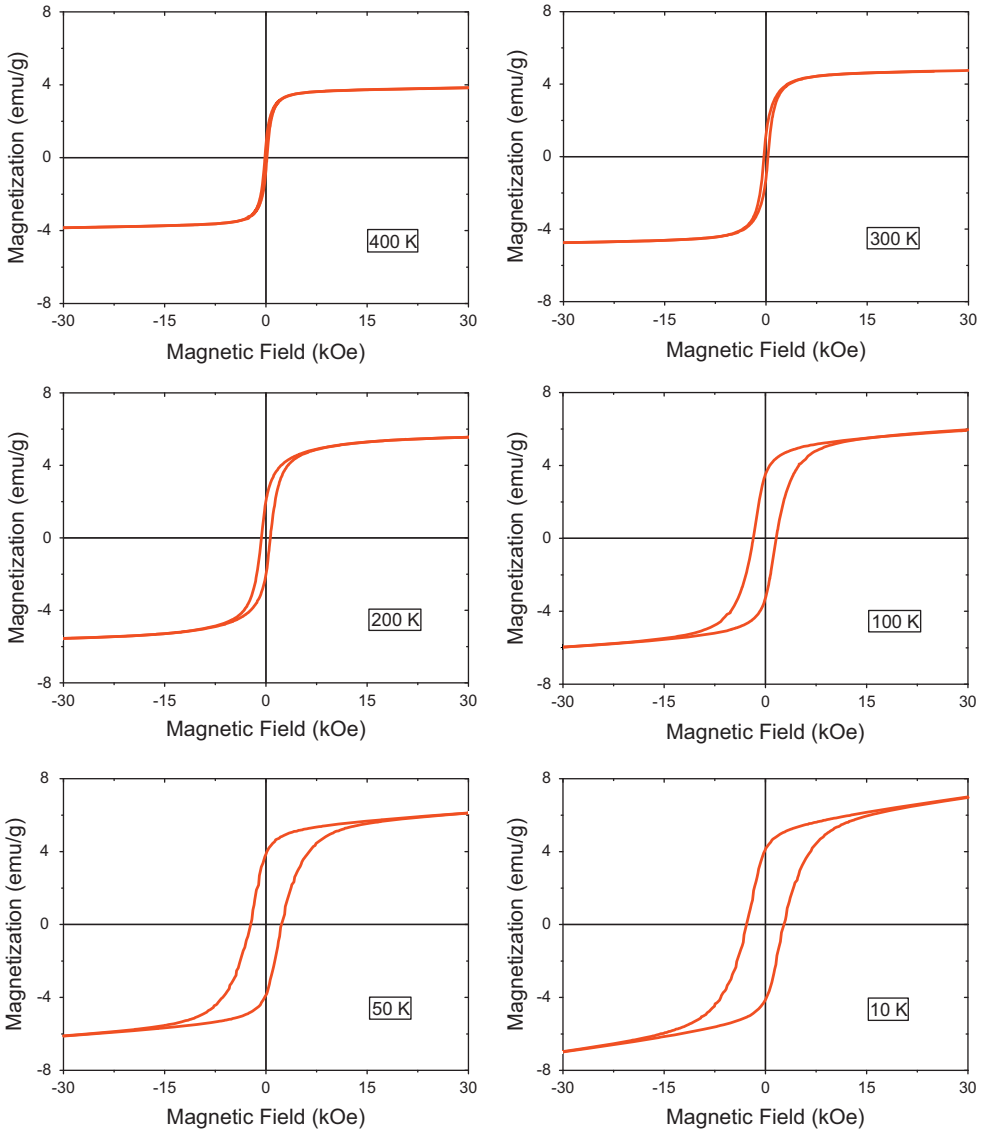


Fig. 5. M–H Hysteresis curves of PANI/$Co_{0.5}Mn_{0.5}Fe_2O_4$ nanocomposite at different temperatures from 10 K to 400 K.

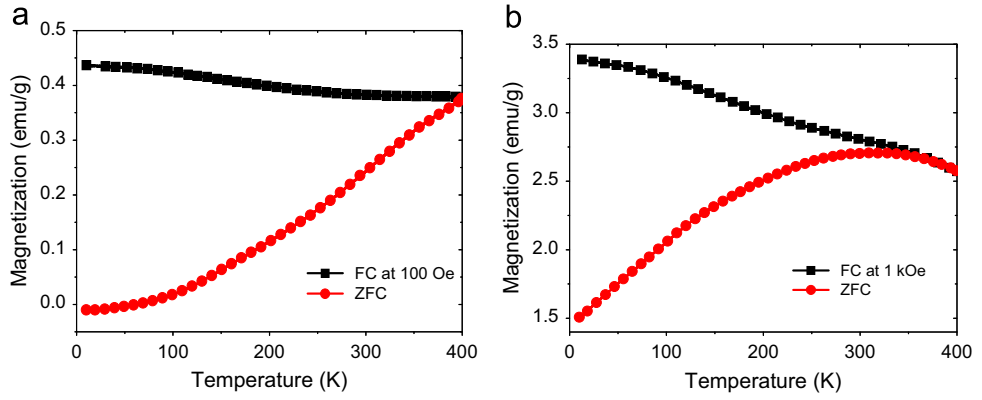


Fig. 6. Temperature dependence of PANI/$Co_{0.5}Mn_{0.5}Fe_2O_4$ nanocomposite of ZFC and FC magnetization curves at different external fields, (a) 100 Oe and (b) 1 kOe.

is related to the blocking of the largest particles [43], while the temperature corresponding to the ZFC maximum ($T_{max}$) is directly proportional to the blocking of particles with average volume [44]. As seen in Fig. 6b, as external field increases from 100 Oe to 1 kOe $T_{sep}$ and $T_B$ shift to low temperatures from 400 K to 325 K.

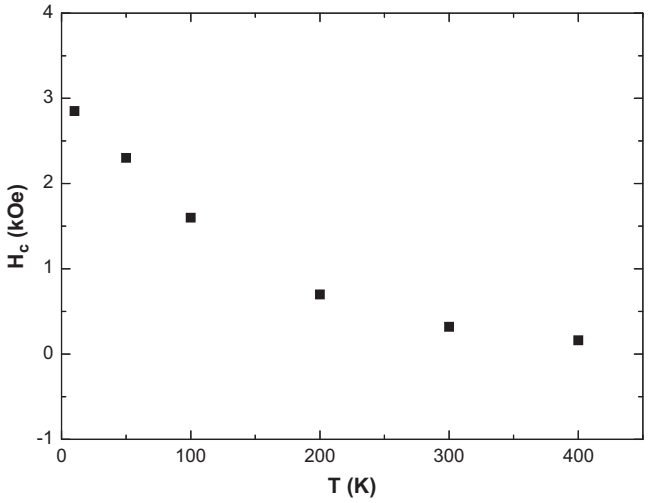


Fig. 7. Temperature dependence of coercivity, $H_c$, of PANI/$Co_{0.5}Mn_{0.5}Fe_2O_4$ nanocomposite.

The difference $T_{sep} - T_{max}$ is a qualitative measure of the width of the energy barrier distribution and thus is proportional to the nanoparticle size distribution. This difference seems to be quite small for our nanoparticles, so we can conclude that particle size distribution of our nanoparticles is rather narrow.

The coercive field, $H_c$, increases almost linearly with decreasing temperature up to 200 K, see Fig. 7. This is due to the fact that magnetocrystalline anisotropy constant ($K_1$), which is directly proportional with $H_c$, increases with decreasing temperature as expressed below:

$$H_c = \pm 2K_1/(\mu_0 M_s)$$

where $\mu_0$ is permeability of the free space.

## 4. Conclusion

The PANI/$Co_{0.5}Mn_{0.5}Fe_2O_4$ nanocomposite has been prepared by in situ polymerization of aniline in the presence of $Co_{0.5}Mn_{0.5}Fe_2O_4$ nanoparticles by ammonium persulphate oxidant in HCl medium. $Co_{0.5}Mn_{0.5}Fe_2O_4$ nanoparticles were prepared via a microwave assisted method and citric acid as the fuel. The average crystallite size was calculated from X-ray line profile fitting as 20 nm. The room temperature magnetization curve of the composite has low coercivity of about 300 Oe which increases with decreasing temperature up to 2.7 kOe. The field cooled and zero field cooled magnetization curves showed that $Co_{0.5}Mn_{0.5}Fe_2O_4$ nanoparticles have superparamagnetic features, which are in a magnetically blocked state at room temperature. The PANI/$Co_{0.5}Mn_{0.5}Fe_2O_4$ nanocomposite seems to be a good candidate as a magnetic filler in MW absorbing materials due to its superparamagnetic nature and presence of conducting polymer layer.

## Acknowledgments

This work is supported by Fatih University under BAP Grant no. P50021104-B.

## References

[1] C. Lucignano, F. Quadrini, L. Santo, Dynamic mechanical performances of polyester—clay nanocomposite thick films, Journal of Composite Materials 42 (2008) 2841–2852.
[2] D. Schlemmer, R.S. Angélica, M.J.A. Sales, Morphological and thermomechanical characterization of thermoplastic starch/montmorillonite nanocomposites, Composite Structures 92 (2010) 2066–2070.
[3] S. Ameen, M.S. Akhtar, G.S. Kim, Y.S. Kim, O.B. Yang, H.S. Shin, Plasma-enhanced polymerized aniline/$TiO_2$ dye-sensitized solar cells, Journal of Alloys and Compounds 487 (2009) 382–386.
[4] B.K. Sharma, N. Khare, S.K. Dhawan, H.C. Gupta, Dielectric properties of nano ZnO–polyaniline composite in the microwave frequency range, Journal of Alloys and Compounds 477 (2009) 370–373.
[5] C. Leng, J. Wei, Z. Liu, J. Shi, Influence of imidazolium-based ionic liquids on the performance of polyaniline–$CoFe_2O_4$ nanocomposites, Journal of Alloys and Compounds 509 (2011) 3052–3056.
[6] K. Lakshmi, H. John, K.T. Mathew, R. Joseph, K.E. George, Microwave absorption, reflection and EMI shielding of PU–PANI composite, Acta Materialia 57 (2009) 371–375.
[7] C. Yang, H. Li, D. Xiong, Z. Cao, Hallow polyaniline/$Fe_3O_4$ microsphere composites: preparation, characterization, and applications in microwave absorption, Reactive and Functional Polymers 69 (2009) 137–144.
[8] R.T. Ma, H.T. Zhao, G. Zhang, Preparation, characterization and microwave absorption properties of polyaniline/$Co_{0.5}Zn_{0.5}Fe_2O_4$ nanocomposite, Materials Research Bulletin 45 (2010) 1064–1068.
[9] Y. Chen, M. Ruan, Y.F. Jiang, S.G. Cheng, W. Li., The synthesis and thermal effect of $CoFe_2O_4$ nanoparticles, Journal of Alloys and Compounds 493 (2010) L36–L38.
[10] G. Bertotti, Connection between microstructure and magnetic properties of soft magnetic materials, Journal of Magnetism and Magnetic Materials 320 (2008) 2436–2442.
[11] C.S. Zhang, L. Yang, Monodispersed nanocrystalline $Co_{1-x}Zn_xFe_2O_4$ particles by forced hydrolysis: synthesis and characterization, Journal of Magnetism and Magnetic Materials 324 (2012) 1469–1472.
[12] O. Caltun, H. Chiriac, N. Lupu, I. Dumitru, P.B. Rao, Journal of Optoelectronics and Advanced Materials 9 (2007) 1158.
[13] J.A. Paulsen, A.P. Ring, C.C.H. Lo, J.E. Synder, D.C. Jiles, Presentation W27-5, American Physician Physical Society, March Meeting Montreal, Quebec, Canada, 2004.
[14] B. Zhou, Y.W. Zhang, C.S. Liao, F.X. Cheng, C.H. Yan, Magnetism and phase transition for $CoFe_{2-x}Mn_xO_4$ nanocrystalline thin films and powders, Journal of Magnetism and Magnetic Materials 247 (2002) 70–76.
[15] S. Kazan, E.E. Tanrıverdi, R. Topkaya, S. Demirci, O. Akman, A. Baykal, B. Aktas, Magnetic properties of triethylene glycol coated $CoFe_2O_4$ and $Mn_{0.2}Co_{0.8}Fe_2O_4$ NP's synthesized by polyol method, Arabian Journal of Chemistry (2012)http://dx.doi.org/10.1016/j.arabjc.2011.12.005.
[16] S. Bhadraa, D. Khastgir, N.K. Singha, J.H. Lee, Progress in preparation, processing and applications of polyaniline, Progress in Polymer Science 34 (2009) 783–810.
[17] A. Garai, A.K. Nandi, Tuning of different polyaniline nanostructures from a coacervate gel/sol template, Synthetic Metals 159 (2009) 757–760.
[18] S.V. Jadhav, Vijaya Puri, Microwave study of chemically synthesized conducting polyaniline on alumina, Synthetic Metals 158 (2008) 883–887.

[19] Q.M. Jia, S.Y. Shan, Y.M. Wang, Recent advances in polyaniline for catalytic applications, Polymeric Materials Science and Engineering 9 (2010) 159.
[20] T. Ahuja, D. Kumar, Recent progress in the development of nano-structured conducting polymers/nanocomposites for sensor applications, Sensors and Actuators B 136 (2009) 275–286.
[21] L.C. Li, H.Z. Qiu, Y.P. Wang, J. Jiang, F. Xu, Preparation and magnetic properties of $Cu_{0.4}Zn_{0.6}Cr_{0.5}Sm_{0.06}Fe_{1.44}O_4$/polyaniline nanocomposites, Journal of Rare Earths 26 (2008) 558–562.
[22] A.O.K. Singh, R.K. Kotnala, A.K. Bakhshi, S.K. Dhawan., Dielectric and magnetic properties of conducting ferromagnetic composite of polyaniline with $\gamma$-$Fe_2O_3$ nanoparticles, Materials Chemistry and Physics 112 (2008) 651–658.
[23] S.H. Hosseini, S.H. Mohseni, A. Asadnia, H. Kerdari, Synthesis and microwave absorbing properties of polyaniline/$MnFe_2O_4$ nanocomposite, Journal of Alloys and Compounds 509 (2011) 4682–4687.
[24] S.P. Lee, Y.J. Chen, C.M. Ho, C.P. Chang, Y.S. Hong, A study on synthesis and characterization of the core–shell materials of $Mn_{1-x}Zn_xFe_2O_4$–polyaniline, Materials Science and Engineering B 143 (2007) 1–6.
[25] G.D. Prasanna, H.S. Jayanna, Preparation, structural, and electrical studies of polyaniline/$ZnFe_2O_4$ nanocomposites, Journal of Applied Polymer Science 120 (2011) 2856–2862.
[26] C.L. Yuan, Y.S. Hong, C.H. Lin, Synthesis and characterization of $(Sr(ZnZr)_xFe_{12-2x}O_{19}$–PANI composites, Journal of Magnetism and Magnetic Materials 323 (2011) 1851–1854.
[27] J. Stejskal, M. Trchova, J. Brodinova, P. Kalenda, S.V. Fedorova, J. Prokes, J. Zemek, Coating of zinc ferrite particles with a conducting polymer, polyaniline, Journal of Colloid and Interface Science 298 (2006) 87–93.
[28] J. Jiang, L. Li, M. Zhu, Polyaniline/magnetic ferrite nanocomposites obtained by in situ polymerization, Reactive and Functional Polymers 68 (2008) 57–62.
[29] S. Kumar, V. Singh, S. Aggarwal, U.K. Mandal, R.K. Kotnala, Bimodal $Co_{0.5}Zn_{0.5}Fe_2O_4$/PANI nanocomposites: synthesis, formation mechanism and magnetic properties, Composites Science and Technology 70 (2010) 249–254.
[30] E.E. Tanrıverdi, A.T. Uzumcu, H. Kavas, A. Demir, A. Baykal, Conductivity study of polyaniline–cobalt ferrite (PANI–$CoFe_2O_4$) nanocomposite, Nano-Micro Letters 3 (2) (2011) 99–107.
[31] Z. Durmus, A. Baykal, H. Kavas, H. Sözeri, Preparation and characterization of polyaniline (PANI)–$Mn_3O_4$ nanocomposite, Physica B 406 (2011) 1114–1120.
[32] T. Wejrzanowski, R. Pielaszek, A. Opalinska, H. Matysiak, W. Łojkowski, K.J. Kurzydłowski, Quantitative methods for nanopowders characterization, Applied Surface Science 253 (2006) 204–208.
[33] R. Pielaszek, Analytical expression for diffraction line profile for polydispersive powders, Applied Crystallography, Proceedings of the XIX Conference, Krakow, Poland, 2003, p. 43.
[34] R.H. Lee, H.H. Lai, J.J. Wang, R.J. Jeng, J.J. Lin, Self-doping effects on the morphology, electrochemical and conductivity properties of self-assembled polyanilines, Thin Solid Films 517 (2008) 500–505.
[35] J. Deng, C. He, Y. Peng, J. Wang, X. Long, P. Li, A.S.C. Chan, Magnetic and conductive $Fe_3O_4$–polyaniline nanoparticles with core–shell structure, Synthetic Metals 139 (2003) 295–301.
[36] S.S. Umarea, B.H. Shambharkara, R.S. Ningthoujam, Synthesis and characterization of polyaniline–$Fe_3O_4$ nanocomposite: electrical conductivity, magnetic, electrochemical studies, Synthetic Metals 160 (2010) 1815–1821.
[37] G.D. Prasannaa, H.S. Jayanna, A.R. Lamani, S. Dash, Polyaniline/$CoFe_2O_4$ nanocomposites: a novel synthesis, characterization and magnetic properties, Synthetic Metals 161 (2011) 2306–2311.
[38] G.V. Duong, N. Hanh, D.V. Linh, R. Groessinger, P. Weinberger, E. Schafler, M. Zehetbauer, Monodispersed nanocrystalline $Co_{1-x}Zn_xFe_2O_4$ particles by forced hydrolysis: synthesis and characterization, Journal of Magnetism and Magnetic Materials 311 (2007) 46–50.
[39] S. Krupicka, P. Nocak, in: E.P. Wohlfarth (Ed.), Ferromagnetic Materials, vol. 3, New Holland, Amsterdam, 1982.
[40] J.M.D. Coey, Noncollinear spin arrangement in ultrafine ferrimagnetic crystallites, Physical Review Letters 27 (1971) 1140–1142.
[41] R.H Kodama, A.E Berkowitz, E.J. McNiff Jr., S Foner, Surface spin disorder in ferrite nanoparticles, Journal of Applied Physics 81 (1997) 5552–5568.
[42] Y. Köseoğlu, M. Bay, M. Tan, A. Baykal, H. Sözeri, R. Topkaya, N. Akdoğan, Magnetic and dielectric properties of $Mn_{0.2}Ni_{0.8}Fe_2O_4$ nanoparticles synthesized by PEG-assisted hydrothermal method, Journal of Nanoparticle Research 13 (2011) 2235–2244.
[43] M.F. Hansen, S. Mørup, Estimation of blocking temperatures from ZFC/FC curves, Journal of Magnetism and Magnetic Materials 203 (1999) 214–216.
[44] J.I. Gittleman, B. Abeles, S. Bozowski, Superparamagnetism and relaxation effects in granular Ni–$SiO_2$ and Ni–$Al_2O_3$ films, Physical Review B 9 (1974) 3891–3897.